

G. R. Liu · G. Y. Zhang · Y. T. Gu · Y. Y. Wang

A meshfree radial point interpolation method (RPIM) for three-dimensional solids

Received: 3 October 2004 / Accepted: 11 January 2005 / Published online: 10 August 2005
© Springer-Verlag 2005

Abstract A meshfree radial point interpolation method (RPIM) is developed for stress analysis of three-dimensional (3D) solids, based on the Galerkin weak form formulation using 3D meshfree shape functions constructed using radial basis functions (RBFs). As the RPIM shape functions have the Kronecker delta functions property, essential boundary conditions can be enforced as easily as in the finite element method (FEM). Numerical examples of 3D solids are presented to verify validity and accuracy of the present RPIM method, and intensive numerical study has been conducted to investigate the effects of some important parameters. It is demonstrated that the present meshfree RPIM is robust, stable, and reliable for stress analysis of 3D solids.

Keywords Numerical analysis · meshfree · meshless · radial point interpolation · 3D solid

1 Introduction

In recent years, a group of meshfree methods have been developed and achieved remarkable progress, such as smooth particle hydrodynamics (SPH) method (Lucy, 1977; Liu and Liu, 2003), diffuse element method (DEM) (Nayroles et al., 1992), element free Galerkin

(EFG) method (Belytschko, 1994) and meshless local Petrov–Galerkin (MLPG) method (Atluri and Zhu, 1998), et al.

The point interpolation method (PIM) (Liu and Gu, 2001a, 2001b, 2001c; Liu, 2002) is a meshfree method developed using Galerkin weak form and shape functions that are constructed based only on a group of nodes arbitrarily distributed in a local support domain by means of interpolation. A global background cell structure is required to evaluate the integration in the Galerkin weak-form. The major advantage of PIM is that the shape functions created possess the Kronecker delta function property, which allows simple enforcement of essential boundary conditions as in the conventional finite element method (FEM). Many numerical techniques and treatments developed in FEM can be largely utilized with minimum modifications. There are two types of PIM shape functions have been used so far with different forms of basis functions: polynomial basis functions (Liu and Gu, 2001c; Liu, 2002) and radial basis functions (RBFs) (Wang and Liu, 2002a, 2002b; Liu, 2002; Liu and Gu, 2005).

PIM using radial basis functions (RBFs) is termed as radial PIM (RPIM). In the RPIM, RBFs are used for constructing shape functions and it has been proved that the moment matrix of the RBF interpolation is usually invertible for arbitrary scattered nodes (Powell, 1992; Schaback, 1994; Wendland, 1998) and there are techniques attempted to overcome the singularity problem (see, e.g., Liu, 2002). RPIM is, however, very stable and robust for arbitrary nodal distributions. There are several advantages of using RBF as basis function in constructing PIM shape functions (Liu, 2002).

- Using RBF can effectively solve the singularity problem of the polynomial PIM, this is also partially because the use of local support domain that contains very small number of nodes.
- RPIM shape functions are stable and hence flexible for arbitrary and irregular nodal distribution.

G. R. Liu (✉) · G. Y. Zhang · Y. T. Gu
Centre for Advanced Computations in Engineering Science (ACES) Department of Mechanical Engineering,
National University of Singapore, 10 Kent Ridge Crescent,
Singapore, 119260.
E-mail: mpeliugr@nus.edu.sg; <http://www.nus.edu.sg/ACES>
Tel.: +65-6874-6481
Fax: +65-67791459

G. R. Liu
SMA Fellow, Singapore-MIT Alliance, Singapore

Y. Y. Wang
Inst High Performance Comp., Singapore

- RPIM shape functions can be easily created for three-dimensional domains, because the only variable is the distance in a RBF.

The RPIM has been successfully applied to 1D and 2D solid mechanics (Gu and Liu, 2001; Liu and Gu, 2001b; Liu and Yan, et al. 2002), plate and shell structures (Liu and Chen, 2001; Liu and Liu, et al. 2002), problems of smart materials (Liu and Dai, et al. 2002), geometrically nonlinear problems (Liu and Dai, et al. 2003), material non-linear problems in civil engineering (Wang et al. 2002), and so on.

In this paper, a 3D RPIM is first formulated based on the Galerkin weak form using locally supported shape functions. Then some important parameters of RPIM are investigated and two numerical examples are presented to demonstrate the efficiency, convergence and accuracy of RPIM for stress analysis of 3D solids.

2 Radial basis point interpolation

Consider a function $u(\mathbf{x})$ defined in a 3D problem domain Ω . The function can be approximated in a local support domain of the point of interest \mathbf{x} with a set of arbitrarily distributed nodes using radial basis function $R_i(\mathbf{x})$ augmented with polynomial basis function $p_j(\mathbf{x})$ (Powell, 1992; Liu, 2002).

$$\begin{aligned} u(\mathbf{x}) &= \sum_{i=1}^n R_i(\mathbf{x})a_i + \sum_{j=1}^m P_j(\mathbf{x})\mathbf{b}_j \\ &= \mathbf{R}^T(\mathbf{x})\mathbf{a} + \mathbf{P}^T(\mathbf{x})\mathbf{b} \end{aligned} \quad (1)$$

where n is the number of RBFs and is also identical to the number of nodes in the local support domain of the point of interest \mathbf{x} , and m is the number of polynomial basis functions. When $m=0$, pure RBFs are used. Otherwise, the RBF is augmented with m terms of polynomial basis functions. Coefficients a_i and b_j are constants yet to be determined.

The polynomial term in Eq. (1) is not always necessary. However, augment of polynomial in RPIM shape functions has the following advantages (Liu, 2002):

1. Adding polynomial term up to the linear order can ensure the C^1 consistency that is needed to pass the standard patch test.
2. In general, adding polynomial can always improve the accuracy of the results, at least no negative effect has been observed for meshfree weak-form methods.

3. Adding polynomial reduces the influence of the shape parameters on the accuracy of the results, and will provide us much more freedom in choosing shape parameters.
4. Adding polynomial can improve the interpolation stability for some RBFs.

In this paper, linear polynomial terms are adopted to augment the RBFs.

In the radial basis function $R_i(\mathbf{x})$, the variable is only the distance between the point of interest (x, y, z) and a node at (x_i, y_i, z_i) ,

$$r = \sqrt{(x - x_i)^2 + (y - y_i)^2 + (z - z_i)^2} \quad (2)$$

There are four types of radial basis functions (RBFs) presented in Table 1, the multi-quadrics (MQ) function, the Gaussian radial function (Exp), the thin plate spline (TPS) function, and the Logarithmic radial basis function. In this paper, the multi-quadrics (MQ) (Hardy, 1990; Liu, 2002) function with real number of parameters is adopted to construct RPIM shape functions and two dimensionless parameters, α_c and q , will be examined in detail in the numerical studies.

In order to determine the constants a_i and b_j , Eq. (1) is enforced to be satisfied at these n nodes in the local support domain, which leads to a set of n equations. The matrix form of these equations can be expressed as

$$\mathbf{U}_e = \mathbf{R}_q \mathbf{a} + \mathbf{P}_m \mathbf{b} \quad (3)$$

where the vector of function values \mathbf{U}_e is

$$\mathbf{U}_e = \{u_1 \quad u_2 \quad \cdots \quad u_n\}^T \quad (4)$$

The moment matrix of RBFs is

$$\mathbf{R}_q = \begin{bmatrix} R_1(r_1) & R_2(r_1) & \cdots & R_n(r_1) \\ R_1(r_2) & R_2(r_2) & \cdots & R_n(r_2) \\ \vdots & \vdots & \ddots & \vdots \\ R_1(r_n) & R_2(r_n) & \cdots & R_n(r_n) \end{bmatrix}_{(n \times n)} \quad (5)$$

The polynomial moment matrix is

$$\mathbf{P}_m = \begin{bmatrix} 1 & x_1 & y_1 & z_1 & \cdots & p_m(\mathbf{x}_1) \\ 1 & x_2 & y_2 & z_2 & \cdots & p_m(\mathbf{x}_2) \\ \vdots & \vdots & \vdots & \vdots & \ddots & \vdots \\ 1 & x_n & y_n & z_n & \cdots & p_m(\mathbf{x}_n) \end{bmatrix}_{(n \times m)} \quad (6)$$

The vector of unknown coefficients for RBFs is

$$\mathbf{a}^T = \{a_1 \quad a_2 \quad \cdots \quad a_n\} \quad (7)$$

Table 1 Typical radial basis functions with dimensionless shape parameters

Name	Expression	Shape parameters (real number)
1. Multi-quadrics (MQ)	$R_i(x, y, z) = (r_i^2 + (\alpha_c d_c)^2)^q$	$\alpha_c \geq 0, q$
2. Gaussian (EXP)	$R_i(x, y, z) = \exp\left[-\alpha_c \left(\frac{r_i}{d_c}\right)^2\right]$	α_c
3. Thin plate spline (TPS)	$R_i(x, y, z) = r_i^\eta$	η
4. Logarithmic	$R_i(x, y, z) = r_i^\eta \log r_i$	η

The vector of unknown coefficients for polynomial is

$$\mathbf{b}^T = \{b_1 \ b_2 \ \cdots \ b_m\} \quad (8)$$

There are $(n + m)$ unknowns in Eq. (3), and here m additional equations need to be added. Following m constraint conditions (Golberg et al. 1999) are applied to obtain the additional unknowns.

$$\sum_{i=1}^n p_j(\mathbf{x}_i) \mathbf{a}_i = \mathbf{P}_m^T \mathbf{a} = 0, \quad j = 1, 2, \dots, m \quad (9)$$

Combining Eqs. (3) and (9) yields the following set of equations in the matrix form

$$\tilde{\mathbf{U}}_e = \begin{bmatrix} \mathbf{U}_e \\ \mathbf{0} \end{bmatrix} = \begin{bmatrix} \mathbf{R}_q & \mathbf{P}_m \\ \mathbf{P}_m^T & \mathbf{0} \end{bmatrix} \begin{Bmatrix} \mathbf{a} \\ \mathbf{b} \end{Bmatrix} = \mathbf{G} \mathbf{a}_0 \quad (10)$$

where

$$\tilde{\mathbf{U}}_e = \{u_1 \ u_2 \ \cdots \ u_n \ 0 \ 0 \ \cdots \ 0\} \quad (11)$$

$$\mathbf{G} = \begin{bmatrix} \mathbf{R}_q & \mathbf{P}_m \\ \mathbf{P}_m^T & \mathbf{0} \end{bmatrix} \quad (12)$$

$$\mathbf{a}_0^T = \{a_1 \ a_2 \ \cdots \ a_n \ b_1 \ b_2 \ \cdots \ b_m\} \quad (13)$$

Because the moment matrix \mathbf{R}_q is symmetric, the matrix \mathbf{G} will also be symmetric. Solving Eq. (10), the unknowns can be obtained as

$$\mathbf{a}_0 = \begin{Bmatrix} \mathbf{a} \\ \mathbf{b} \end{Bmatrix} = \mathbf{G}^{-1} \tilde{\mathbf{U}}_e \quad (14)$$

Substituting Eq. (14) into Eq. (1) leads to

$$u(\mathbf{x}) = \{ \mathbf{R}^T(\mathbf{x}) \ \mathbf{P}^T(\mathbf{x}) \} \mathbf{G}^{-1} \tilde{\mathbf{U}}_e = \tilde{\Phi}(\mathbf{x}) \tilde{\mathbf{U}}_e \quad (15)$$

where

$$\begin{aligned} \tilde{\Phi}^T(\mathbf{x}) &= \{ \mathbf{R}^T(\mathbf{x}) \ \mathbf{P}^T(\mathbf{x}) \} \mathbf{G}^{-1} \\ &= \{ \phi_1(\mathbf{x}) \ \phi_2(\mathbf{x}) \ \cdots \ \phi_n(\mathbf{x}) \\ &\quad \phi_{n+1}(\mathbf{x}) \ \cdots \ \phi_{n+m}(\mathbf{x}) \} \end{aligned} \quad (16)$$

Finally, the RPIM shape functions $\Phi(\mathbf{x})$ are obtained as

$$\Phi^T(\mathbf{x}) = \{ \phi_1(\mathbf{x}) \ \phi_2(\mathbf{x}) \ \cdots \ \phi_n(\mathbf{x}) \} \quad (17)$$

Eq. (15) can be rewritten as

$$u(\mathbf{x}) = \Phi^T(\mathbf{x}) \mathbf{U}_e = \sum_{i=1}^n \phi_i u_i \quad (18)$$

The derivatives of $u(\mathbf{x})$ can be easily obtained as

$$u_{,l}(\mathbf{x}) = \Phi_{,l}^T(\mathbf{x}) \mathbf{U}_e \quad (19)$$

where l denotes the coordinates x , y or z . A comma designates a partial differentiation with respect to the indicated spatial coordinate that follows.

3 Global weak-form for three dimensional solids

Consider the static problem defined in the 3D domain Ω boundary by Γ . The standard partial differential equa-

tion and boundary conditions for a 3D solid mechanics problem can be given as the follows (Timoshenko and Goodier, 1970).

Equilibrium equation:

$$\mathbf{L}^T \sigma + \mathbf{b} = 0 \quad \text{on } \Omega \quad (20)$$

Natural boundary condition:

$$\sigma \cdot \mathbf{n} = \bar{\mathbf{t}} \quad \text{on } \Gamma_t \quad (21)$$

Essential boundary condition:

$$\mathbf{u} = \bar{\mathbf{u}} \quad \text{on } \Gamma_u \quad (22)$$

where \mathbf{L} is differential operator; $\sigma^T = \{ \sigma_{xx} \ \sigma_{yy} \ \sigma_{zz} \ \tau_{xy} \ \tau_{yz} \ \tau_{zx} \}$ is the stress vector, $\mathbf{u}^T = \{ u \ v \ w \}$ is the displacement vector, $\mathbf{b}^T = \{ b_x \ b_y \ b_z \}$ is the body force vector, $\bar{\mathbf{t}}$ is the prescribed traction on the natural boundaries, $\bar{\mathbf{u}}$ is the prescribed displacement on the essential boundaries, and \mathbf{n} is the vector of unit outward normal at a point on the neutral boundary.

The unconstrained Galerkin weak form of Eq. (20) is posed as the follows (see, e.g., Liu, 2002)

$$\int_{\Omega} (\mathbf{L} \delta \mathbf{u})^T (\mathbf{D} \mathbf{L} \mathbf{u}) \, d\Omega - \int_{\Omega} \delta \mathbf{u}^T \mathbf{b} \, d\Omega - \int_{\Gamma_t} \delta \mathbf{u}^T \bar{\mathbf{t}} \, d\Gamma = 0 \quad (23)$$

where \mathbf{D} is the matrix of elastic constants. For 3D isotropic solids, we have

$$\mathbf{D} = \frac{E(1-\nu)}{(1+\nu)(1-2\nu)} \begin{bmatrix} 1 & & & & & & \\ \frac{\nu}{1-\nu} & 1 & & & & & \\ \frac{\nu}{1-\nu} & \frac{\nu}{1-\nu} & 1 & & & & \\ 0 & 0 & 0 & \frac{1-2\nu}{2(1-\nu)} & & & \\ 0 & 0 & 0 & 0 & \frac{1-2\nu}{2(1-\nu)} & & \\ 0 & 0 & 0 & 0 & 0 & \frac{1-2\nu}{2(1-\nu)} & \end{bmatrix} \quad (24)$$

where E and ν are Young's modulus and Poisson's ratio respectively.

It should be mentioned that Eq. (23) is a weak-form defined over the global problem domain Ω . Although theoretically the constrained Galerkin weak form should be used to enforce the global compatibility, it has been found that the unconstrained Galerkin weak form works well with RPIM shape functions (Liu, 2002). Hence, the unconstrained Galerkin weak form is used in this work.

Substituting Eq. (18), the approximations of $u(\mathbf{x})$, into Eq. (23) yields

$$\mathbf{K} \mathbf{u} = \mathbf{f} \quad (25)$$

where \mathbf{K} is the stiffness matrix

$$\mathbf{K}_{ij} = \int_{\Omega} \mathbf{B}_i^T \mathbf{D} \mathbf{B}_j \, d\Omega \quad (26)$$

in which \mathbf{B} is a strain matrix

$$\mathbf{B}_i = \begin{bmatrix} \phi_{i,x} & 0 & 0 \\ 0 & \phi_{i,y} & 0 \\ 0 & 0 & \phi_{i,z} \\ \phi_{i,y} & \phi_{i,x} & 0 \\ 0 & \phi_{i,z} & \phi_{i,y} \\ \phi_{i,z} & 0 & \phi_{i,x} \end{bmatrix} \quad (27)$$

In Eq. (25), \mathbf{f} is the nodal force vector given by

$$\mathbf{f}_i = \int_{\Gamma_i} \phi_i \bar{\mathbf{t}} d\Gamma + \int_{\Omega} \phi_i \mathbf{b} d\Omega \quad (28)$$

The numerical procedure of RPIM for 3D problems is listed as follows:

1. Looping over background cells to determine all Gauss points to find out its location and weight.
2. Looping over Gauss points for integration of Eq. (18)
 - a. Determine the support domain for specified Gauss point and select neighboring nodes based on a defined criterion,
 - b. Compute shape function and its derivatives for each Gauss point,
 - c. Evaluate stiffness and load at each Gauss point,
 - d. Assemble the contribution of each Gauss point to form system equation.
3. Enforcing essential (displacement) boundary conditions.
4. Solving the system equation to obtain nodal displacements.
5. Computing stress components.

4 Analysis of shape parameters through function fitting

The solutions obtained using the RPIM may first depend on the quality of its shape functions. Hence, in this section, the interpolation errors using RBF shape functions are examined through fitting a given function. The MQ-RBF is employed for interpolation and linear polynomial terms are included in the following studies.

In order to perform the interpolation, a local support domain must be taken into account. In this paper, two different models of the support domain are examined. Model-1 of support domain is defined as a spherical domain centered at the point of interest \mathbf{x} (which is often a quadrature point). Then the field nodes within the sphere would be adopted in the local support domain for this point of interest. The dimension of the support domain is naturally defined by the radii of the sphere, which is determined as the follows

$$d_s = \alpha_s d_c \quad (29)$$

where α_s is dimensionless size of the support domain, and d_c is the nodal spacing near the point of interest \mathbf{x} . If the nodes are uniformly distributed, d_c is simply the distance between two neighboring nodes. In the case where the nodes are non-uniformly distributed, d_c can be defined as an ‘‘average’’ nodal spacing in the support domain (see, e.g., Liu, 2002).

As Model-2 of support domain is concerned, the number of field nodes in the local support domain would be predefined, i.e., n . Then according to the different distances between the field nodes and the point of interest \mathbf{x} , the n nodes which are the nearest to the point of interest \mathbf{x} are adopted in the support domain. The results of using these two models will be presented in the following studies.

In the analysis of function fitting, a domain of $(x, y, z) \in [0, 1] \times [0, 1] \times [0, 1]$ is considered and 729 uniformly distributed field nodes with a constant nodal distance $d_c = 0.125$ are adopted to represent the domain. A total of 512 regularly distributed points of $(x, y, z) \in [0.05, 0.95] \times [0.05, 0.95] \times [0.05, 0.95]$ are used as interpolation points.

Because the linear function in 3D is reproduced exactly when linear polynomial terms are included in Eq. (1) (Liu, 2002), a harmonic function of 3D is considered, i.e.,

$$f(x, y, z) = \sin x \cos y \sin z \quad (30)$$

The first-order partial derivative with respect to x is

$$f_{,x}(x, y, z) = \cos x \cos y \sin z \quad (31)$$

The approximated values of the field function and the first derivative with x for each interpolation point \mathbf{x} can be obtained using interpolation as the follows:

$$\tilde{f}(\mathbf{x}) = \mathbf{\Phi}(\mathbf{x}) \mathbf{F}_s = \sum_{i=1}^n \phi_i f_i \quad (32)$$

$$\tilde{f}_{,x} = \frac{\partial \mathbf{\Phi}(\mathbf{x})}{\partial x} \mathbf{F}_s = \sum_{i=1}^n \frac{\partial \phi_i}{\partial x} f_i \quad (33)$$

where ϕ_i is the RPIM-MQ shape function, and n is the number of field nodes used in the support domain. Vector \mathbf{F}_s collects the true nodal function values for these n field nodes, and f_i is the function value for the i th field node.

The following norms are used as error indicators.

$$e = \frac{1}{N} \sum_{i=1}^N \left| \frac{\tilde{f}_i - f_i}{f_i} \right| \quad (34)$$

$$e' = \frac{1}{N} \sum_{i=1}^N \left| \frac{\tilde{f}_{,x}^i - f_{,x}^i}{f_{,x}^i} \right| \quad (35)$$

where N is the total number of the interpolation nodes.

4.1 Shape parameters of the RPIM-MQ

The effects of two shape parameters, q and α_c , in the MQ-RBF are first studied. In the process of this study, Model-1 of support domain is adopted and $\alpha_s = 3.0$ is fixed in the study.

In the study of the effect of q , $\alpha_c = 4.0$ is fixed. The average fitting errors e obtained for different values of q are plotted in Fig. 1. It can be found that a more accurate

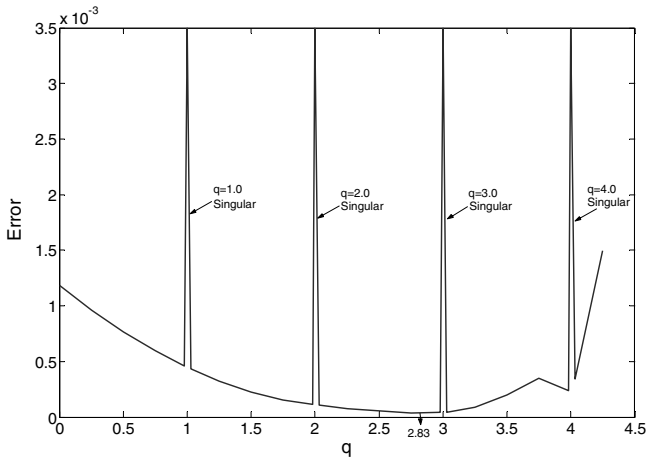


Fig. 1 Error in function fitting using RPIM-MQ shape functions with different q (MQ-RBF augmented with linear polynomials is used with shape parameter $\alpha_c = 4.0$ and Model-1 of the support domain is adopted with $\alpha_s = 3.0$)

result can be obtained when the value of q varies between 1 and 3 (but not 1, 2 and 3). When $q > 4.0$, the fitting error is found very large due to the badly conditioned moment matrix. However, if the value of q is identical to 1.0, 2.0, 3.0 and 4.0, the RPIM-MQ will fail due to the singularity of the moment matrix. In addition, if q is too close to 1.0, 2.0 or 3.0, the condition number of interpolation matrix of RPIM will become bigger, the moment matrix will be nearly singular and the results are not stable any more. The preferred value of parameter q is close to 1.0, 2.0 or 3.0, but not equal to these values. Therefore, in using RPIM shape functions, one has to strike a good balance between accuracy and stability.

Figure 2 shows the effect of parameter α_c on function fitting accuracy. For comparison, two curves of function fitting errors obtained using $q = 1.03$ and $q = 2.83$ are plotted in the figure. The value, $q = 1.03$, which is found by Wang and Liu (2002b), performs the best for most computational problems. The other value, $q = 2.83$, is found leads to the best result in the previous study of parameter q . It can be found, when $\alpha_c > 3.0$, the value of the fitting error is very small and changes little with respect to either the change of parameter α_c or q .

4.2 Convergence studies

In the convergence study, Model-1 of the support domain is employed, $q = 1.03$ $\alpha_c = 4.0$ $\alpha_s = 3.0$ are fixed. The convergence curves with respect to nodal refinement are plotted in Fig. 3. Note that in Fig. 3, h is actually the nodal spacing d_c defined in Eq. (29), which is simply the distance between two neighboring nodes as the fields nodes are regularly and evenly distributed in this function fitting test. It can be found that RPIM has obtained very good convergence rates for fitting both function and its first-order derivative. However, the convergence process of the first-order partial derivative with x is not as stable as the process of the function.

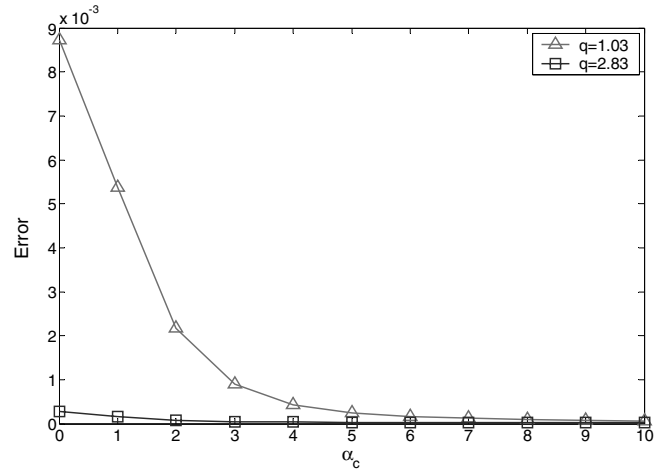


Fig. 2 Error in function fitting using RPIM- MQ with different α_c (MQ-RBF augmented with linear polynomials is used and Model-1 of the support domain is adopted with $\alpha_s = 3.0$)

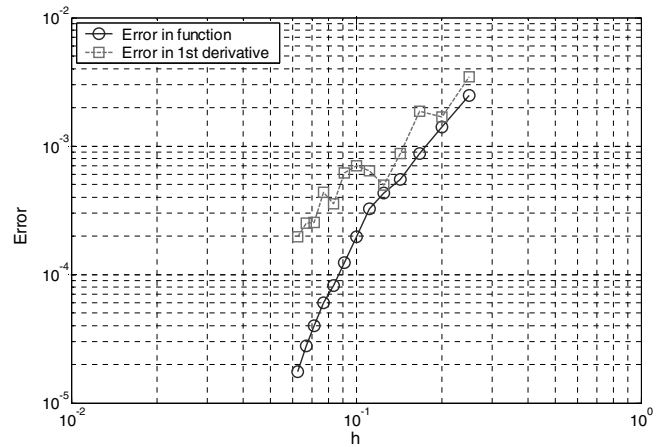


Fig. 3 Errors in function fitting using RPIM-MQ shape functions (MQ-RBF augmented with linear polynomials is used with shape parameter: $q = 1.03$ and $\alpha_c = 4.0$; Model-1 of the support domain is adopted with $\alpha_s = 3.0$)

It should be noted here that the interpolation error is only one part of total error in a meshfree method in solving a problem of computational mechanics. The studies of shape parameters presented in this section are only to check the interpolation quality and the reproducibility of using RPIM-MQ shape functions. The accuracy will be also studied in the following sections in the analysis of actual problems of computational mechanics.

5 Numerical experiments of 3D elasticity problems

In order to validate the present method, the RPIM is used for displacement and stress analysis of 3D solids. The units are all taken as international standard units and the material adopted is linear elastic with $E = 3.0 \times 10^7$ and $\nu = 0.3$ in this paper.

5.1 A cantilever beam

A 3D cantilever beam as shown in Fig. 4 is studied to benchmark the present method. The left end of the beam is fixed and the right end is subjected to a parabolically distributed downwards traction. As the beam is relatively thin, a plane stress problem can be considered to yield the analytical solution (Timoshenko and Goodier, 1970). This analytical solution is adopted as the reference solution in our numerical study.

The displacement components of the analytical solution are given by

$$u_x = -\frac{py}{6EI} \left[(6L - 3x)x + (2 + \nu) \left(y^2 - \frac{D^2}{4} \right) \right] \quad (36)$$

$$u_y = \frac{p}{6EI} \left[3\nu y^2(L - x) + (4 + 5\nu) \frac{D^2 x}{4} + (3L - x)x^2 \right] \quad (37)$$

where the moment of the inertia I of the beam is given by $I = D^3/12$.

The stress components corresponding to above displacements are

$$\sigma_x = -\frac{p(L - x)y}{I} \quad (38)$$

$$\sigma_y = 0 \quad (39)$$

$$\sigma_{xy} = \frac{p}{2I} \left[\frac{D^2}{4} - y^2 \right] \quad (40)$$

The parameters are taken as $P = -1000$, $L = 50$, $D = 10$ and $B = 1$ in the study of this numerical example.

5.1.1 Effects of parameters and the dimension of the support domain

In the following studies, the cantilever beam is regarded as a 3D solid, and RPIM is used to obtain numerical solutions. The effects of parameters q , α_c and the dimension of the support domain on the displacements results of the cantilever are then investigated. The problem domain is represented by 1122 regularly distributed field nodes, and 500 hexahedron-shaped background cells are used for numerical integration. In each background cell, $4 \times 4 \times 4$ Gauss points are employed. The error indicator is defined as the follows:

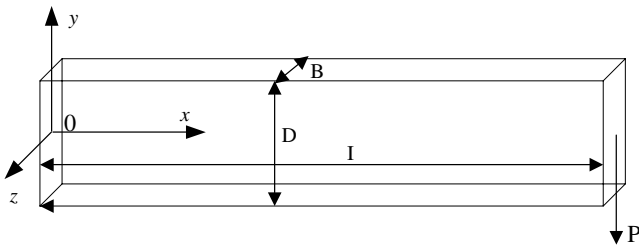


Fig. 4 A 3D cantilever beam subjected to a parabolic traction at the free end

$$e_v = \frac{1}{N} \sum_{i=1}^N \left| \frac{V_i^{\text{RPIM}} - V_i^{\text{analytical}}}{V_i^{\text{analytical}}} \right| \quad (41)$$

where V_i denotes the displacement in y -direction of the i th node and N is the number of total field nodes.

- Effect of parameter q
In this investigation, α_c is fixed at 4.0, Model-1 of the support domain is adopted and α_s is fixed at 3.0. Errors defined in Eq. (41) for different values of q are computed and plotted in Fig. 5. It can be found that when q in the range of 1.0 – 3.0 (but not 1, 2, and 3), the value of error is very small and error changes very little with respect to the change of q . The figure also shows that for this particular case, $q = 3.28$ leads to the best result, and, when $q > 3.28$, the error will significantly increase because of the big condition number of the moment matrix.
- Effect of parameter α_c
The effects of α_c is studied for a wide range of 1.0 – 10.0 with Model-1 of the support domain employed and α_s fixed at 3.0. Errors for different values of α_c are plotted in Fig. 6. For comparison, two values of parameter q are employed. One value is 1.03, and the other one is 3.28, which has been found producing the best result in the previously study. The figure shows that when $\alpha_c > 3.0$, we can get a more accurate and stable result, and the difference between the results, obtained using $q = 1.03$ and $q = 3.28$ respectively, is very little.
- Effect of the dimensions of support domains
In the process of this study, $q = 1.03$ and $\alpha_c = 4.0$ are fixed. Two curves obtained using two models of the support domain respectively are plotted in Fig. 7. Considering that using too many nodes in the support domain will cause time consuming, about the use of 20 – 70 nodes gives a better result for these two

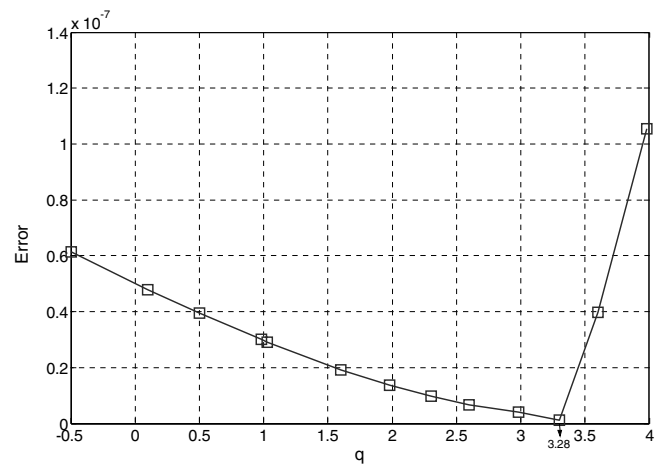


Fig. 5 Influence of parameter q on the displacement results obtained using RPIM-MQ. (Error is defined by Eq. (41); a total 1122 regularly distributed field nodes and 500 hexahedron-shaped back ground cells are used; MQ-RBF augmented with linear polynomials is used with shape parameter $\alpha_c = 4.0$ and Model-1 of the support domain is adopted with $\alpha_s = 3.0$)

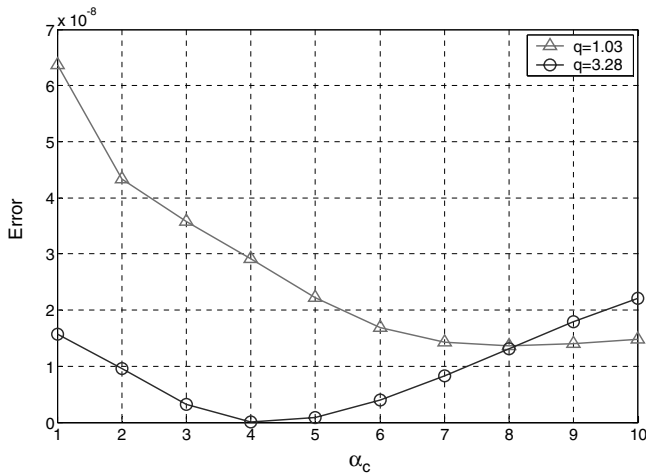


Fig. 6 Influence of α_c on the displacement results obtained using RPIM-MQ with $q = 1.03$, $q = 3.28$ and different α_c (Error is defined by Eq. (41); a total 1122 regularly distributed field nodes and 500 hexahedron-shaped back ground cells are used; MQ-RBF augmented with linear polynomials is used and Model-1 of the support domain is adopted with $\alpha_s = 3.0$)

models of the support domain. The figure also shows that Model-2 over performs Model-1. This can be explained as the follows. By using Model-1, fewer nodes will be adopted in the support domain when the point of interest is located near or at the boundaries. Using Model-2, there will not be such a problem, as we always use a fixed number of nearest nodes.

In the following studies, $q = 1.03$ and $\alpha_c = 4.0$ are adopted which have been found perform well in most computational problems that have been investigated so far (Liu, 2002; Wang and Liu, 2002b); Model-2 is employed based on our studies previously.

5.1.2 Results of the cantilever beam

In the 3D RPIM analysis of the cantilever beam, both a regular nodal distribution and an irregular nodal distribution, shown respectively in Figs. 8 and 9, are employed. For the regular nodal distributed model, there are totally 2223 field nodes and 1344 hexahedron-shaped background integration cells, in each tetrahedron cell, $4 \times 4 \times 4$ Gauss points are used to evaluate the stiffness matrix; for the irregular nodal distributed model, 1620 field nodes and 4447 tetrahedron-shaped background integration cells are used, 11 Gauss points are employed in each tetrahedron cell in the process of integration. As Model-2 of support domain is employed, 55 and 52 field nodes are involved in the support domains for regular and irregular nodal distribution respectively.

Figures 10–12 show the comparisons between the analytical solutions and the RPIM results, in which Fig. 10 shows the comparison for displacement in y -direction along the neutral axis, Fig. 11 for the normal stress and Fig. 12 for shear stress. All these plots show

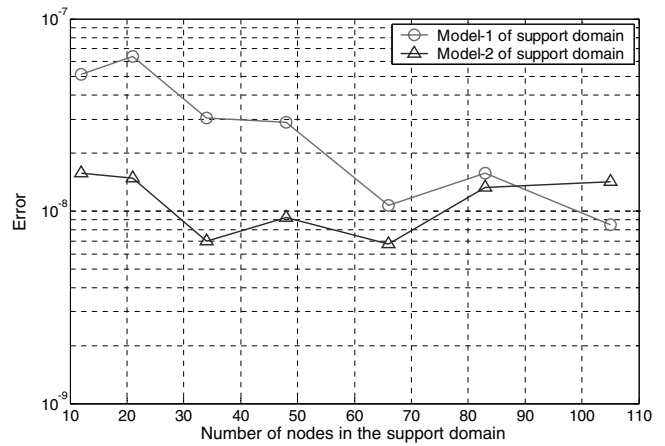


Fig. 7 Influence of the dimensions of support domains on the RPIM-MQ (Error is defined by Eq. (41); a total 1122 regularly distributed field nodes and 500 hexahedron-shaped back ground cells are used; MQ-RBF augmented with linear polynomials is used with shape parameter $q = 1.03$, and $\alpha_c = 4.0$)

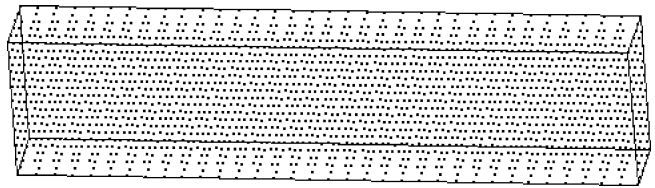


Fig. 8 Regular nodal distribution for the cantilever (A total of 2223 regular field nodes and 1344 hexahedron-shaped background cells are used)

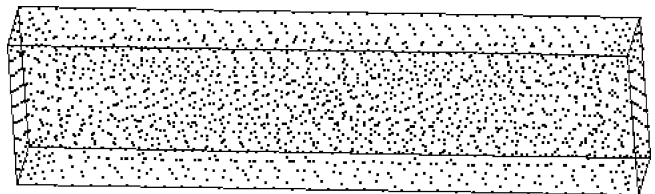


Fig. 9 Irregular nodal distribution for the cantilever (A total of 1620 irregular field nodes and 4447 tetrahedron-shaped background cells are used)

that the results obtained using RPIM in 3D for both regular and irregular nodal distributed models are in good agreement with the analytical solutions. Another conclusion is that, the regularity of nodal distribution has little effect on the result of the RPIM.

5.2 An axletree base

In this example, the displacement analysis of an axletree base is studied using the present 3D-RPIM code. As shown in Fig. 13, the axletree base is symmetric about the y - z plane, subjected to a uniformly distributed force along a line and fixed in the locations of four lower cylindrical holes and the bottom plane. The value of the

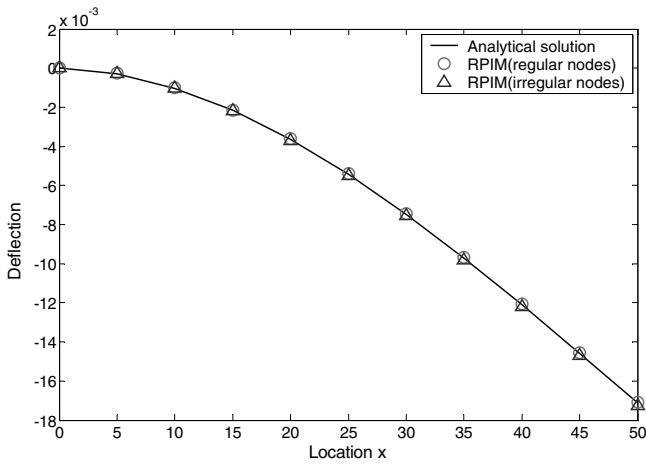


Fig. 10 Displacement (u_y) distribution along the neutral axis (MQ-RBF augmented with linear polynomials is used with shape parameter $q = 1.03$ and $\alpha_c = 4.0$; Model-2 of the support domain is adopted, 52 and 55 field nodes are involved in the support domain for regular and irregular nodal distribution respectively)

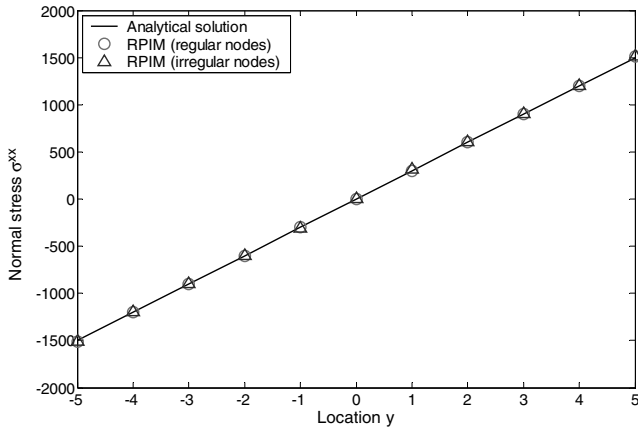


Fig. 11 Normal stress distribution along the line of $x = L/2, z = 0.0$ (MQ-RBF augmented with linear polynomials is used with shape parameter $q = 1.03$ and $\alpha_c = 4.0$; Model-2 of the support domain is adopted, 52 and 55 field nodes are involved in the support domain for regular and irregular nodal distribution respectively)

uniformly distributed force is 5000. Numerical results at point K and two lines (Line 1 and Line 2) will be examined in our study.

First, for the displacement distribution along Line 1, Line 2 and at point K, a reference solution is obtained using FEM software ANSYS with a very fine mesh of high order elements (ten-node tetrahedron element). Then the displacement results are obtained using the RPIM and ANSYS (four-node tetrahedron element is employed) with exactly the same distribution of nodes for comparison. In the process of this study, the background cell distribution of the RPIM model is also the same as the element distribution of ANSYS model.

Figures 14 and 15 show the displacement distribution along Line 1 and Line 2 obtained using the RPIM and

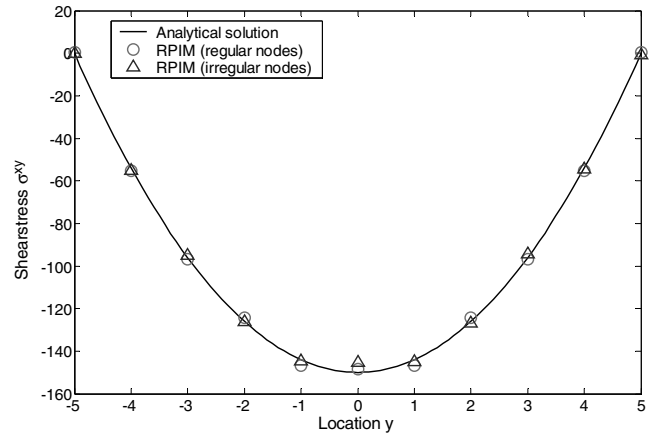


Fig. 12 Shear stress distribution along the line of $x = L/2, z = 0.0$ (MQ-RBF augmented with linear polynomials is used with shape parameter $q = 1.03$ and $\alpha_c = 4.0$; Model-2 of the support domain is adopted, 52 and 55 field nodes are involved in the support domain for regular and irregular nodal distribution respectively)

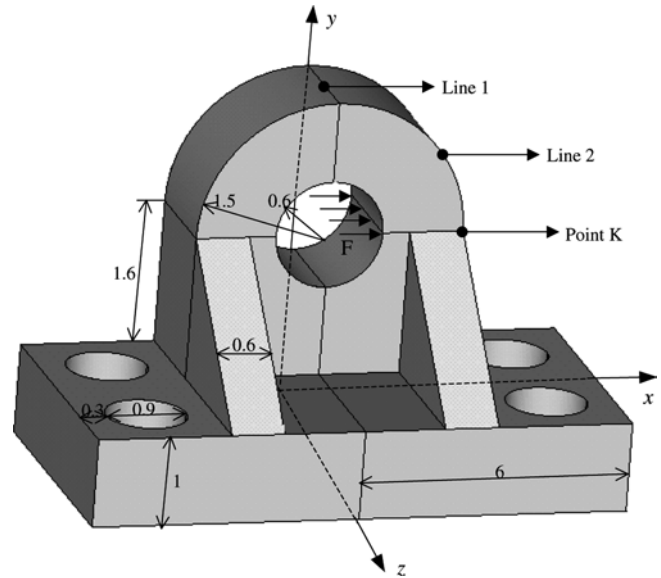


Fig. 13 An axletree base

ANSYS respectively under the same condition (totally 4571 irregular distributed field nodes and 20561 tetrahedron-shaped background cells). It can be found that, the results obtained using the RPIM closely matches the corresponding reference solution and are much closer to the reference solutions than that obtained using ANSYS adopting a linear element.

Finally, a comparison of the convergence studies between the RPIM and ANSYS is carried out. Point K located as shown in Fig. 14 is selected as the reference point. Figure 16 shows that both the RPIM and the FEM software ANSYS have a good convergence rate, but the RPIM can get more accurate results than ANSYS using a linear element.

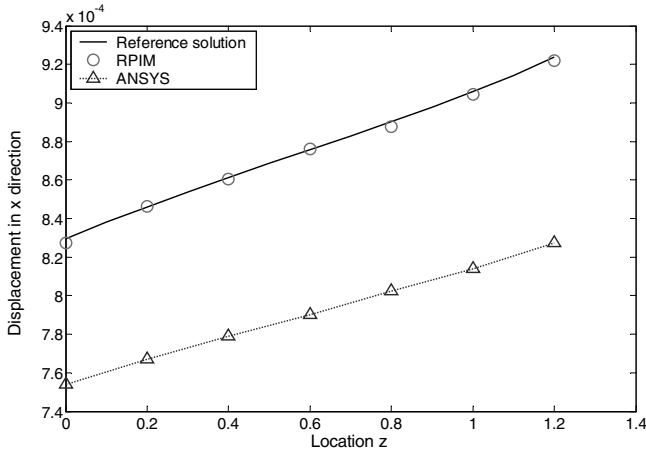


Fig. 14 Distribution of the displacement u_x along Line 1 (The results are obtained using the RPIM and ANSYS under the same condition: totally 4571 irregular distributed nodes and 20561 tetrahedron-shaped cells. For the RPIM: MQ-RBF augmented with linear polynomials is used with shape parameter $q = 1.03$ and $\alpha_c = 4.0$; Model-2 of the support domain is adopted and 29 field nodes are involved in the support domain. For the ANSYS, linear tetrahedron element is adopted.)

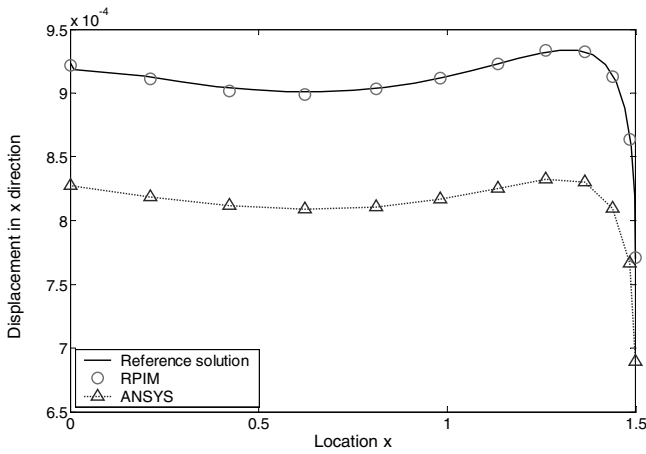


Fig. 15 Distribution of the displacement u_x along Line 2 (The results are obtained using the RPIM and ANSYS under the same condition: totally 4571 irregular distributed nodes and 20561 tetrahedron-shaped cells. For the RPIM: MQ-RBF augmented with linear polynomials is used with shape parameter $q = 1.03$ and $\alpha_c = 4.0$; Model-2 of the support domain is adopted and 29 field nodes are involved in the support domain. For the ANSYS, linear tetrahedron element is adopted.)

6 Conclusions

A meshfree radial point interpolation method (RPIM) for three-dimensional solids is presented in this paper. The radial basis functions augmented with polynomial are used to construct shape functions based on a 3D local support domain. Therefore, the essential boundary conditions can be implemented as easy as in the conventional FEM. Based on the work done on 1D and 2D problems, the RPIM for 3D are formulated

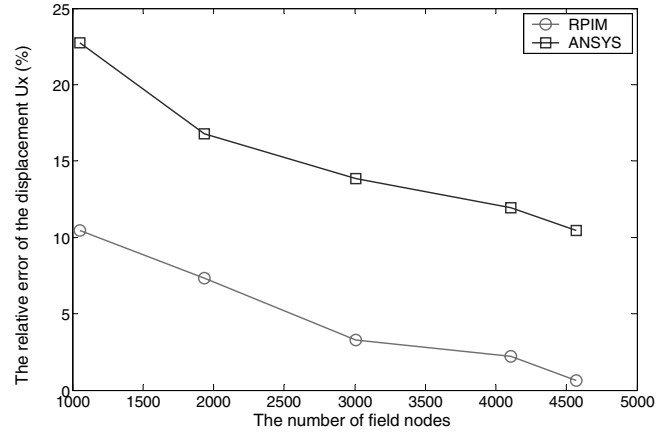


Fig. 16 A comparison of convergence between the RPIM and FEM software ANSYS (The results are obtained using the RPIM and ANSYS under the same condition: the same number of nodes and cells. For the RPIM: MQ-RBF augmented with linear polynomials is used with shape parameter $q = 1.03$ and $\alpha_c = 4.0$; Model-2 of the support domain is adopted and 29 field nodes are involved in the support domain. For the ANSYS, linear tetrahedron element is adopted.)

and coded in this work. Some important parameters are investigated in detail and two numerical examples of 3D solids are studied using the present 3D-RPIM.

Base on the study conducted, following conclusions can be drawn:

1. The RPIM shape functions constructed using RBF augmented with polynomial possess the following features:
 - The RPIM shape functions are capable of reproducing what is contained in the basis, which is essential for any numerical method to produce accurate solution.
 - The RPIM shape functions have a good convergence capability. This allows the error of the approximation of function that is sufficiently smooth to approach zero when the nodal spacing is reduced sufficiently small.
2. Based on the study of function fitting and the numerical example, the remarks of the effect of some shape parameters are noted as follows:
 - For parameter q , the value in the range of 1.0–3.0 (but not 1, 2, and 3) is recommended for 3D problems, and $q = 1.03$ is a robust choice, which is also consistent with the findings from 2D-RPIM studies.
 - For parameter α_c , when its value is bigger than 3.0, we can obtain a better result and $\alpha_c = 4.0$ is a robust and consistent choice in the RPIM.
 - For the two models of the support domain presented in this paper, Model-2 performs better for most 3D problems especially when the geometry of the domain is complicated. For Model-1, $\alpha_s = 3.0$ is recommended; for Model-2, 20–70 nodes in the local support domain are preferred.

3. The comparison study of the axletree has shown that the RPIM has better accuracy than the linear FEM.

In a summary, we state that the RPIM is a very stable, robust and reliable numerical method for stress analysis of 3D solids.

References

- Atluri SN, Zhu T (1998) A new meshless local Petrov-Galerkin (MLPG) approach in computational mechanics. *Comput Mech* 22:117–127
- Belyschko T, Lu YY, Gu L (1994) Element – free Galerkin methods. *Int J Numer Meth Eng* 37:229–256
- Golberg MA, Chen CS, Bowman H (1999) Some recent results and proposals for the use of radial basis functions in the BEM. *Eng Anal Boundary Elements* 23:285–296
- Gu YT, Liu GR (2001) A local point interpolation method for static and dynamic analysis of thin beams. *Comput Methods Appl Mech Eng* 190:5515–5528
- Hardy RL (1990) Theory and applications of the multiquadrics – biharmonic method (20 years of discovery 1968–1988). *Comput. Math. Appl.* 19: 163–208
- Liu GR (2002) *Mesh Free Methods: Moving Beyond the Finite Element Method*. CRC Press, New York, USA
- Liu GR, Chen XL (2001) A mesh-free method for static and free vibration analyses of thin plates of complicated shape. *J Sound Vib* 241(5):839–855
- Liu GR, Dai KY, Lim KM, Gu YT (2002) A point interpolation meshfree method for static and frequency analysis of two-dimensional piezoelectric structures. *Comput Mech* 29(6):510–519
- Liu GR, Dai KY, Lim KM (2003) A meshfree method for analysis of geometrically nonlinear problems (submitted)
- Liu GR, Gu YT (2001a) A local point interpolation method for stress analysis of two-dimensional solids. *Struct Eng Mech* 11(2):221–236
- Liu GR, Gu YT (2001b) A local radial point interpolation method (LR-PIM) for free vibration analyses of 2-D solids. *J Sound Vib* 246(1):29–46
- Liu GR, Gu YT (2001c) A point interpolation method for two-dimensional solids. *Int J Numer Methods Eng* 50:937–951
- Liu GR, Gu YT (2005) *An introduction to meshfree methods and their programming*. Springer, Dordrecht, The Netherlands
- Liu GR, Liu MB (2003) *Smoothed particle hydrodynamics – A meshfree practical method*, World Scientific, Singapore
- Liu GR, Yan L, Wang JG, Gu YT (2002) Point interpolation method based on local residual formulation using radial basis functions. *Struct Eng Mech* 14(6):713–732
- Liu L, Liu GR, Tan VBC (2002) Element free method for static and free vibration analysis of spatial thin shell structures. *Comput Methods Appl Mech Eng* 191(51–52):5923–5942
- Lucy L (1977) A numerical approach to testing the fission hypothesis. *Astron J* 82:1013–1024
- Nayroles B, Touzot G, Villon P (1992) Generalizing the finite element method: Diffuse approximation and diffuse elements. *Comput Mech* 10:307–318
- Powell MJD (1992) The theory of radial basis function approximation in 1990. In: Light FW (ed) *Advanced in numerical analysis*, pp. 303–322
- Schaback R (1994) Approximation of polynomials by radial basis functions. In: Laurent PJ, Mehaute Le, Schumaker LL (Eds) *Wavelets, images and surface fitting*, Wellesley, MA pp 459–466
- Timoshenko SP, Goodier JN (1970) *Theory of Elasticity* (3rd edn). McGraw-Hill, New York
- Wang JG, Liu GR (2002a) A point interpolation meshless method based on radial basis functions. *Int J Numer Meth Eng* 54(11):1623–1648
- Wang JG, Liu GR (2002b) On the optimal shape parameters of radial basis functions used for 2-D meshless methods. *Comput Methods Appl Mech Eng* 191:2611–2630
- Wang JG, Liu GR, Lin P (2002) Numerical analysis of Biot’s consolidation process by radial point interpolation method. *Int J Solids Struct* 39(6):1557–1573
- Wendland H (1998) Error estimates for interpolation by compactly supported radial basis functions of minimal degree. *J Approximation Theory* 93:258–396